Momentum dependence of local fields in solids

C. Tarrio and S. E. Schnatterly
Jesse Beams Laboratory of Physics, University of Virginia, Charlottesville, Virginia 22901
(Received 1 August 1991)

We report measurements of microscopic local fields in four polycrystalline solids obtained in two different manners. In N_2, the local field shows a striking increase with momentum out to our maximum measured value of 1.1 Å^{-1}, while in O_2 the local field increases at low momentum and reaches a maximum at 0.75 Å^{-1}. In Ar, the dielectric constant, which is directly related to the local-field strength, shows a sharp increase but reaches a maximum and begins to decrease at high momentum. In Kr, the dielectric constant shows only a small increase before reaching a maximum. For the cubic cases, we find reasonable agreement with point-dipole calculations. These results suggest that in many cubic materials, the local-field strength near the Brillouin-zone boundary may be up to a factor of 4 stronger than the Clausius-Mossotti value at the zone center.

INTRODUCTION

The existence of local-field effects, in which the field experienced at a particular atom differs from the macroscopic field due to induced dipoles on other atoms in the system, has long been known. The original discussions, based on considering metallic spheres embedded in a dielectric medium, led to the familiar Clausius-Mossotti and Lorentz-Lorenz relations over 100 years ago.[1–4] Later density-dependent index-of-refraction measurements on the rare-gas solids proved the validity of the Clausius-Mossotti relation in cubic solids.[5]

More recently the possibility of momentum dependence of local effective fields was addressed by Nagel and Witten.[6] Their calculations, based on point dipoles on the three cubic lattices, found a striking momentum dependence of the local-field strength. The present authors recently measured this effect in fcc N_2 and found a large increase in the local-field strength with wave vectors out to the zone boundary.[7]

Introduction of a wave-vector dependence is equivalent to the introduction of a spatial dependence in the applied electric field. Thus any system in which there is a large electric-field gradient requires nonzero wave vectors to describe the field. This is the case near an interface or point defect. An electron that is localized in such a system experiences the local field rather than the macroscopic field. Systems of current interest in which this is the case include semiconductor nanostructures and defect and dopant diffusion near surfaces.

In the present study we report in more detail our inelastic electron scattering (IES) measurements on solid N_2, Ar, Kr, and O_2. The first three crystallize in the fcc structure, while β-O_2 is orthorhombic. In the cases of N_2 and O_2, we obtain the local-field factor by direct comparison of our solid-state spectra to analogous spectra obtained from the free molecules. For Ar and Kr, we base our estimates of the local-field strength on assumptions about the behavior of the valence excitons.

BACKGROUND

A dielectric material in the presence of an applied electric field develops a polarization field, $\mathbf{P}=\chi\mathbf{E}$, where χ is the susceptibility. The field at a point inside a solid can be thought of as a sum of the macroscopic field, the polarization field, and a contribution from the near neighbors. In the zero wave-vector limit in a cubic or random structure the sum of the contributions due to dipoles induced on the near neighbors is zero. The internal field is then the sum of the macroscopic field plus the polarization field, $(4\pi/3)\mathbf{P}=(4\pi/3)\chi\mathbf{E}_{\text{loc}}$, where $\mathbf{E}_{\text{loc}}$ is the local field. This leads to an enhancement in the local field by a factor of $1/[1-(4\pi/3)\chi]$ relative to the macroscopic applied field. Recalling the relationships between the susceptibility and the dielectric constant, $\epsilon=1+4\pi\chi$, and the atomic or molecular polarizability, $\chi=n\alpha$, where n is the density and α is the polarizability, we arrive at the Clausius-Mossotti relation:

$$\epsilon=1+\frac{4\pi n\alpha}{1-(4\pi/3)}n\alpha\ . \tag{1}$$

An electric field with finite wave vector causes phases of the dipole moments of the system to vary with position. If this is the case, the contribution of the near-neighbor atoms does not vanish even for cubic lattices. Nagel and Witten[6] modified the Clausius-Mossotti relation by including a momentum-dependent local-field factor $B(q)$:

$$\epsilon(q,\omega)=1+\frac{4\pi n\alpha(\omega)}{1-B(q)n\alpha(\omega)}\ , \tag{2}$$

where q is the momentum and we have introduced a frequency ω. The local-field factor $B(q)$ is related to the dipole sum:

$$B(q)=4\pi+\sum_j{}'\cos(\mathbf{q}\cdot\mathbf{r}_j)\frac{3[\hat{\mathbf{q}}\cdot(\mathbf{R}-\mathbf{r}_j)]^2-(\mathbf{R}-\mathbf{r}_j)^2}{|\mathbf{R}-\mathbf{r}_j|^5}\ . \tag{3}$$

In this expression, **R** is the position of the atom at which the dipole field is being evaluated, $\mathbf{r}_j$ is the position of another atom in the solid, **q** is the momentum, $\hat{\mathbf{q}}$ is a unit vector parallel to **q**, and the prime denotes excluding the origin from the sum. $B(q)$ can be calculated directly by evaluating the sum over a cluster of sufficient size. The results for the three principal axes of the fcc structure, shown in Fig. 1, indicate an increase in $B(q)$ by as much as a factor of 3 with momentum for some crystal directions, and only a small increase or even a decrease in other cases. In all cases, the value of $B(q)$ approaches the zero-momentum value of $4\pi/3$ as expected from the Clausius-Mossotti relation. It must be noted that the size of the local field depends on the local-field factor and the susceptibility. Thus, large local fields are not only a result of a large $B(q)$ but also of large polarizabilities and high densities. Moreover, atoms or molecules with larger polarizabilities also have larger radii, and would be expected to have behavior that deviates significantly from the predictions of the point-dipole approximation.

Results for polycrystalline structures, such as those we have measured, can be approximated by calculating $B(q)$ in several directions and averaging the appropriate measured quantity. We have done this to allow comparison to our measured data. For example, we have evaluated $B(q)$ in the [110], [320], [210], [310], [410], [510], and [100] directions in the (100) plane. Four directions were calculated for the (111) plane and 11 directions for the (110) plane. The measured quantities (the dielectric constant or field strength) were then calculated for each direction and the appropriate average taken, assuming that our samples had randomly oriented crystallites.

DATA ACQUISITION AND ANALYSIS

In inelastic electron scattering we measure the response of the sample to the electric displacement vector of the fast electrons. The cross section for inelastic scattering is proportional to

$$\frac{d^2\sigma}{d\omega d\Omega} \propto \frac{1}{q^2}\mathrm{Im}\left[-\frac{1}{\epsilon(q,\omega)}\right], \tag{4}$$

where $\hbar q$ is the momentum transfer and $\hbar\omega$ is the energy of the excitation. Using the Kramers-Kronig relation,

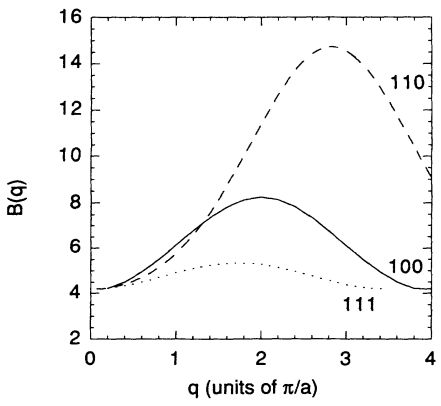

FIG. 1. $B(q)$ for three principal axes in the fcc structure.

$$\mathrm{Re}\left[\frac{1}{\epsilon(q,\omega)}\right] = 1 + \frac{2}{\pi}\int_0^\infty \frac{\omega'\mathrm{Im}\left[-\frac{1}{\epsilon(q,\omega')}\right]}{(\omega')^2-\omega^2}d\omega' \tag{5}$$

we can evaluate both the real and imaginary parts of the dielectric function as a function of both momentum and energy.

Data were measured using the IES accelerator described in Ref. 8. Primary beam energy was 285 keV with resolution 70–130 meV. Energy losses from 2 to 60 eV were covered using a precision programmable power supply. Transverse momentum transfer was delivered by high-voltage capacitor plates. Momentum transfers of 0.07 to 1.3 Å^{-1} were covered with a resolution of 0.04 to 0.07 Å^{-1}.

Thin-film samples were condensed onto 50–100-Å carbon and 250-Å aluminum substrates held at about 30 K by a low-temperature sample mount described in Ref. 9. Ultrapure gases flowed over the substrates at pressures of 10^{-6} to 3×10^{-5} Torr for 1–6 min, resulting in films about 100–2000 Å thick. Deposition rates and sample thicknesses were varied. Background pressure in the sample chamber was $<10^{-9}$ Torr. The possibility of contamination was investigated by leaving uncoated substrates cold and measuring spectra until plating of background gases could be detected, a period of over a week. Therefore, the substrates were warmed up every few days and a fresh sample was deposited. The rare-gas solids have band gaps larger than the atmospheric gases, and we were not able to detect impurity signals in the band gap of any of the Kr or Ar spectra, indicating that contamination had not occurred in those samples. Results reported here represent data obtained on at least three samples of each gas. The order in which spectra were measured was not systematic, that is, measurements did not proceed from low momentum to high momentum or vice versa. Diffraction measurements indicated polycrystalline samples with the following lattice parameters: N_2, 5.65 Å; Ar, 4.73 Å; Kr, 5.69 Å, in agreement with accepted values.[10] O_2 results were difficult to interpret, but appeared orthorhombic, indicating the β phase, which is the stable phase at about 30 K.

Each measured spectrum is the sum of the sample and substrate contributions. Since C and Al are both metals, and the solid gases are wide-band-gap insulators, an estimate of the substrate contribution can be obtained by scaling the spectrum of the substrate below the absorption threshold of the sample. C and Al spectra were measured over broad energy ranges at the appropriate q values for each measured sample spectrum. Spectra also contain multiple-scattering events, in which a single fast electron scatters more than once in the sample, and a kinematic weighting factor, which is energy dependent. These effects are removed using algorithms of Fields[11] and Livins, Aton, and Schnatterly.[12] The amount of multiple scattering removed and the final scale of a spectrum are determined using constraints on the low-frequency dielectric constant and the oscillator strength sum rule. Oscillator strengths of 10.4 electrons per molecule for N_2, 12.5 for O_2, and 8.5–9 electrons per atom for Ar and Kr

were used in carrying out this analysis.[13] Low-momentum dielectric constants were obtained from polarizability measurements for N_2 (Ref. 14) and from solid-state measurements for O_2, Ar, and Kr.[5] The determination of the dielectric constant at higher momenta is discussed in the next section.

Higher-momentum spectra also contain thermal-diffuse scattering, a type of multiple scattering in which a fast electron scatters quasielastically at high momentum from a phonon, then inelastically from a low-momentum electronic excitation. In the case of the rare-gas solids, the energies of the fundamental exciton peaks increase with momentum at a high enough rate that we can detect thermal-diffuse scattering in the data. These contributions can be subtracted using a method similar to the substrate subtraction. In the case of N_2 and O_2, however, the excitations are molecular in nature, and thus nondispersive. We therefore estimate the maximum momentum at which the contribution of thermal-diffuse scattering remains small enough to be ignored based on previous measurements on solids of similar molecular weight, and have limited our study to less than about 1.1 Å^{-1}.

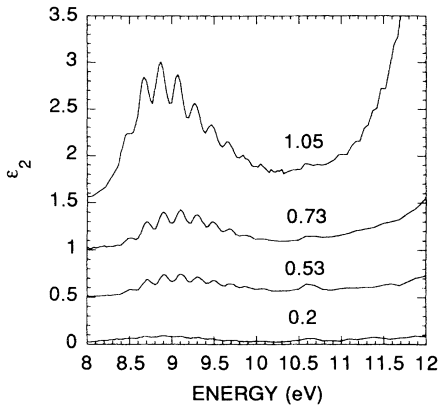

FIG. 2. ϵ_2 spectra of N_2 at a variety of momentum transfers; momentum transfers in Å^{-1} are indicated near each curve.

DETERMINATION OF LOCAL FIELDS

The most direct way to evaluate the local-field strength is a comparison of the intensities of appropriate spectral features between the gas phase, in which local fields are negligible, and the solid state. This requires that, in the energy range covered, the only differences between the gas phase and solid state be the local fields. N_2 provides such a comparison. The Lyman-Birge-Hopfield transition, the $a\,^1\Pi_g \leftarrow X\,^1\Sigma_g^+$ molecular excitation, centered around 9.1 eV, is an electric quadrupole transition in both the gas and the cubic solid, and thus, being dipole forbidden, exhibits a striking increase in intensity with increasing momentum. It is spatially localized and also isolated in energy from other transitions. The momentum-dependent behavior in the free molecule is well documented in the literature,[15–17] and so provides a good gas-phase comparison for our data. We have evaluated ϵ_2 spectra using a Kramers-Kronig analysis of our measured data. Figure 2 shows our results for several momentum values.

The gas-phase IES cross section is related to the imaginary part of the molecular polarizability.[18] Gas-phase measurements are reported in terms of the generalized oscillator strength, $f(q)$, as a function of momentum.[15–17] Since in the gas we have $\epsilon_1 \simeq 1$, we can compare gas-phase results directly to our momentum-dependent oscillator strengths obtained from ϵ_2:

$$N_{\text{eff}}(q)=\frac{2}{\pi\omega_p^2}\int_{\omega_{\text{ex}}}\omega\epsilon_2(q,\omega)d\omega\ , \tag{6}$$

where N_{eff} is the oscillator strength, ω_p is an effective plasma frequency, and the integral is over the contribution of the transition. We can evaluate the square of the electric-field enhancement directly from the oscillator strength ratio:

$$\frac{E_{\text{loc}}^2(q,\omega_{\text{peak}})}{E_{\text{mac}}^2(q,\omega_{\text{peak}})}=\frac{N_{\text{eff}}(q)}{f(q)} \tag{7a}$$

$$=\frac{1}{\{[1-B(q)]n\alpha(\omega_{\text{peak}})\}^2}\ . \tag{7b}$$

Due to weak magnetic dipole transitions above 9.5 eV, we have evaluated our oscillator strengths by fitting a series of seven Gaussians to the lowest vibrational levels for each of our spectra. We have evaluated the oscillator strength of the entire transition based on the contributions of the three most intense peaks, assuming a Poisson distribution.

Our oscillator strengths obtained from ϵ_2 are strongly dependent on the assumption of the low-frequency dielectric constant, which is in turn dependent on our assumption of $B(q)$. For the same raw spectrum a larger input value of $\epsilon_1(q,0)$ shifts oscillator strength to lower energies in ϵ_2. For this reason we have used an iterative procedure to determine $B(q)$. For each spectrum we have assumed an input value of $B(q)$, and used the molecular polarizability and Eq. (2) to obtain $\epsilon_1(q,0)$. We go through our analysis procedure to obtain $\epsilon_2(q,\omega)$, $N_{\text{eff}}(q)$, and an output value of $B(q)$ based on comparison with the data in Ref. 15. The procedure is iterated until the input and output values of $B(q)$ are the same.

The oscillator strengths obtained from this procedure are shown in Fig. 3, along with the data of Ref. 15. The strengths obtained for the solid are higher at every q value. In addition, the solid state and free molecule strengths exhibit a different behavior with momentum. The gas-phase strength initially increases quadratically with momentum, as would be expected from the matrix element, then eventually increases less than quadratically. In the solid, however, the initial increase is also approximately quadratic, but at intermediate momentum, the increase is more than quadratic, indicating that some process is enhancing the transition in the solid. The solid-state oscillator strength does not extrapolate to zero at zero momentum, suggesting that some additional oscillator strength due to odd-parity phonon coupling or disor-

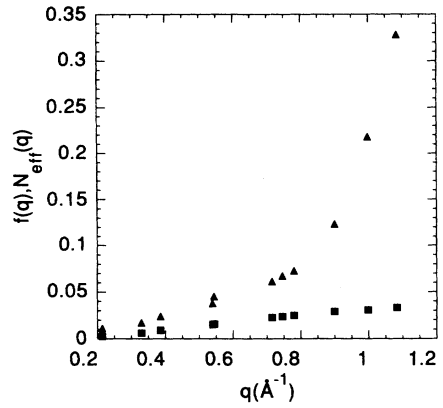

FIG. 3. Oscillator strengths of N_2 for the free molecule (squares, Ref. 15) and the cubic solid (triangles).

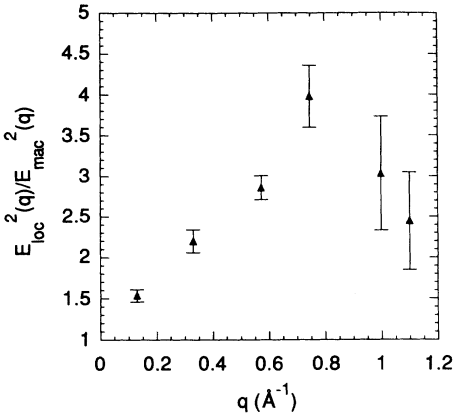

FIG. 5. Local-field strength in solid O_2.

der, which introduces some dipole character to the transition, is present.[19] This admixture should be momentum independent. Therefore we have subtracted 0.0088 electron from our data to evaluate $B(q)$. The value of 0.0088 was chosen to allow the local-field factor to extrapolate smoothly to the known value of $4\pi/3$ at $q=0$. The values of the square of the local-field enhancement obtained from the oscillator strength ratios and our calculated averages for the three planes in the fcc structure are shown in Fig. 4.

We have used an identical procedure for O_2. In the free molecule, the Schumann-Runge transition $B^3\Sigma_u^- \leftarrow X^3\Sigma_g^-$ is dipole allowed, and its oscillator strength decreases with momentum for the free molecule.[20] In the molecule the Schumann-Runge transition has very little vibrational structure and appears as a broad peak more than 1 eV wide and centered at 8.45–8.75 eV.[20] We have used two Gaussians to fit our data, which include a solid-state transition at 7.4 eV and the Schumann-Runge transition at 8.8 eV. The resulting local-field enhancement obtained from comparison of our data to those in Ref. 20 is shown in Fig. 5. It must be noted that ϵ_1 is varying by 10–30 % in the energy range of the transition, and we have used an average value of ϵ_1 to obtain our assumed value of $n\alpha_1(\omega_{\text{peak}})$. This leads to small uncertainties at low q, where the variation is about 10%, but to larger uncertainties at high q, where the variation is larger.

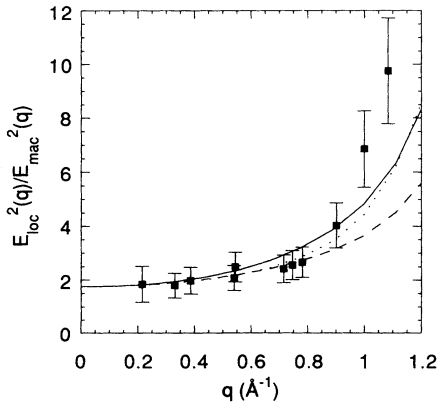

FIG. 4. Local-field field strength as a function of momentum for N_2 (squares) with averages for three crystal planes as described in the text: solid line, (100) plane; dashed line, (110) plane; dotted line, (111) plane.

Since Ar and Kr have complicated excitonic behavior not present in the gas phase, direct comparison to the spectra of the free atoms cannot be made. Therefore we have had to make some assumptions about the momentum-dependent excitonic behavior. Both Ar and Kr have localized valence bands of p character and extended conduction bands of s character at the Γ point, where the absorption threshold is.[21]

In the case of Ar, we base our assumptions on the oscillator strengths and spin-orbit splitting of the $p_{3/2}$ and $p_{1/2}$ excitons. In $\text{Im}(-1/\epsilon)$ the ratio of the oscillator strength of the exciton arising from the $p_{3/2}$ band to that of the $p_{1/2}$ band is about 0.05, and the spin-orbit splitting is 0.6 eV. In the free atom the oscillator strengths of the transitions are about equal, while the spin-orbit splitting is 0.2 eV.[22] While a small difference in behavior between the free atom and the solid is expected, differences such as these are unusual. On the other hand, if we examine the behavior of ϵ_2 in the solid at low q, we find a spin-orbit splitting of 0.19 eV and an oscillator strength ratio of about unity, in agreement with optical experiments.[23,24] Therefore, the difference in behavior is due to the values of ϵ_1 in the region of the transition. The intensity ratio between the $p_{1/2}$ and $p_{3/2}$ excitons changes rapidly with the values of ϵ_1 in this energy range. Because the structure is so sharp, it is affected strongly by the assumed value of $\epsilon(\omega=0)$ through the Kramers-Kronig relation, thus the assumed value of $B(q)$, which contributes to the value of $\epsilon_1(0)$, changes both the oscillator strength ratio and spin-orbit splitting in the transition. Therefore, we have varied $B(q)$ for each q value until the strength ratio and spin-orbit splitting are about equal to our low-momentum results, which are consistent with optical measurements.[22] Figure 6 shows ϵ_2 spectra obtained at $q=0.4$ Å^{-1} assuming three different input values of $B(q)$. As can be seen, the resulting ϵ_2 spectrum is very

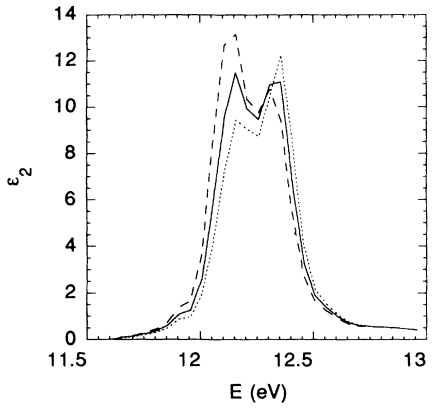

FIG. 6. ϵ_2 spectra of Ar in the energy region near the fundamental exciton at $q=0.4$ Å^{-1}, assuming different $B(q)$ values: 6.0, dashed line; 6.5, solid line; and 7.0, dotted line.

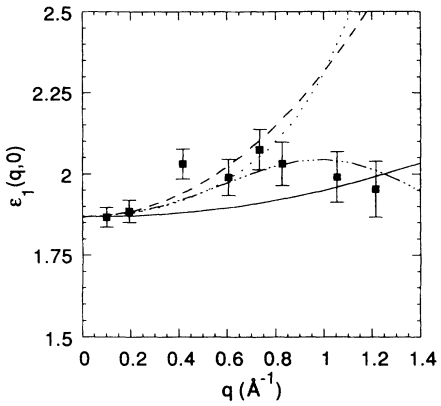

FIG. 8. $\epsilon_1(q,0)$ in solid Kr (squares) with averages for the three crystal planes; notation as in Fig. 4. Chain lines are for the (110) plane with form factors as described in the text.

sensitive to our choice of $\epsilon_1(q,0)$. The results for $\epsilon_1(q,0)$ are presented in Fig. 7.

We have used similar assumptions to obtain $B(q)$ for solid Kr. Although ϵ_1 in the region of the $4p$ excitons is not nearly as rapidly varying as in solid Ar, the behavior of the $p_{3/2}$ exciton peak in ϵ_2 is strongly dependent on our choice of $\epsilon_1(\omega\rightarrow 0)$. To evaluate $B(q)$, we have assumed that the oscillator strength ratio remains constant as in the case of Ar, however in Kr, we found a low-q oscillator strength ratio in ϵ_2 of about 1.3. This is a little higher than the value of 1.1 found in reflectivity experiments.[23,24] Values of $\epsilon_1(q,0)$ obtained in this manner are shown in Fig. 8.

Uncertainties arise in all of the steps in our data analysis. In each solid uncertainties are present due to substrate subtraction, multiple-scattering removal, and the Kramers-Kronig analysis. The latter two are especially uncertain at high momentum. In N_2 most of the uncertainty at low momentum is due to odd-parity phonons, disorder, and substrate subtraction. At higher momentum, where the Schumann-Runge transition has increased in intensity, these become smaller. In the high-momentum region in both N_2 and O_2, the greatest uncertainties are in our analysis procedures and the fact that ϵ_1 in the region of the transitions studied is varying by as much as 10% in N_2 and 30% in O_2. In Ar the dominant contribution to uncertainty is thermal-diffuse scattering, which must be removed from the higher-momentum spectra. This, coupled with the weakness of the $p_{3/2}$ exciton in the energy-loss spectrum, introduces large uncertainties at intermediate to high momentum. The Kr ϵ_2 spectrum is much less sensitive to the value of $\epsilon_1(q,0)$, so the dominant source of uncertainty is simply determining this value precisely. We have included error bars in our figures based on these considerations.

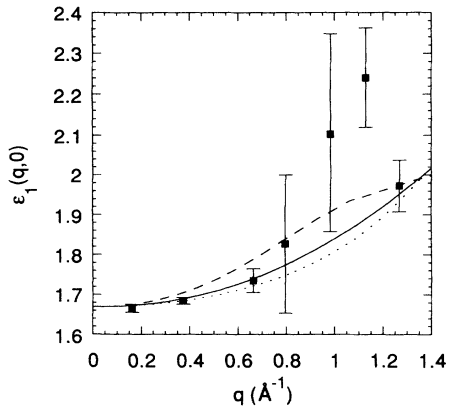

FIG. 7. $\epsilon_1(q,0)$ in solid Ar (squares) with averages for the three crystal planes; notation as in Fig. 4.

DISCUSSION

Results for the four different materials obtained using different methods of evaluating $B(q)$ are fairly different. All of our samples showed diffraction rings of each principal axis direction, thus we may expect our data to be well described by an average over orientation, however none of our results for the three cubic solids are described particularly well by simple averages over orientation. The N_2 data follow all three of the plane averages well until high momentum, where the data are greater than any of the averages. At high momentum the data follow the results for several directions in the (100) plane, however, indicating possibly some preferential orientation. The data for Ar become highly uncertain as q is increased, as discussed above.

The calculations were made for point dipoles. In real solids the sizes of the atoms or molecules can have a large effect on the local field. Thus we may expect a larger atom such as Kr to have behavior which deviates significantly from the calculations. In Fig. 7 we show dashed lines which include a Lorentzian form factor in $\alpha(q)$, which approximates the deviation from the point-dipole approximation. The form factor we have used is $F(q)=1/(1+aq^2r_0^2)$, where r_0 is the atomic or molecular radius and a is a constant. In Fig. 7 we have included

curves for $a=0.1$ and 0.05 for q in the 110 direction.

Momentum-dependent measurements are sensitive to the degree of localization of transitions we have used to determine the local fields. The transitions in N_2 and O_2 are nondispersive, and thus extremely localized. In the rare-gas solids, however, the excitons disperse measurably, indicating that they are more extended. It is the variation with q of ϵ_1 which we are using in this case to probe the local field. What counts then is the degree of localization of the valence electrons which largely determine ϵ_1. The more extended exciton states are simply being used as a probe, allowing us to evaluate $\epsilon_1(q)$.

For primitive cubic lattices such as these, $B(q)$ is periodic in the reciprocal lattice when q is oriented along a high-symmetry direction. For other directions of $\mathbf{q}$, $B(q)$ has no apparent simple periodicity. In every case there is an upper limit to the value of $B(q)$, given by $B(q)n\alpha(q)<1$. For example, in N_2 this requires $B(q)<18$, a condition met by our evaluations and measurements.

As mentioned earlier, the magnitude of the local-field enhancement is related to both $B(q)$ and the susceptibility. The susceptibilities of the materials we have measured vary between 0.043 for Ar and 0.055 for N_2 and Kr, and the maximum local-field factors vary from 7 for Kr to 13.5 for Ar. The ratio of the local field to the macroscopic field is $1/[1-B(q)n\alpha]$. To find the magnitude of this effect, we have evaluated this for each solid. The largest effect is in N_2, in which the local-field enhancement near the zone boundary is a factor of about 3 greater than the macroscopic field. In Kr, on the other hand, the enhancement is only 1.6 over the macroscopic field. The results for Ar and O_2 are between these results.

Perhaps a more familiar way to think of fields is in real space. The present results can be expressed in real space by a Fourier transform of the results in momentum space. The macroscopic electric field around a point charge in q space is $E(q)=2\pi^2/q$, and the local field is the product of the macroscopic field and the enhancement factor. We can transform this into real space by using our calculated values of $B(q)$ with a form factor, or by fitting curves to our measured electric-field enhancements. We found that a curve of the form $(a+bq^3)/(c+dq^5)$ described the shape of $E(q)$ for each solid adequately. The integrals were performed over 200 periods, and a damping term was added due to the instability of the integral. The results show that the enhancement in the electric field approaches unity at $r\rightarrow 0$ and $r\rightarrow\infty$, and shows a broad peak at about 1.2 Å in Kr, 1.5 Å in Ar and N_2, and 2.0 Å in O_2. The enhancement at the peak is about 1.8 in O_2 and Kr and about 2.3 in Ar and N_2. As an example, we show the electric-field enhancement in O_2 in real space in Fig. 9.

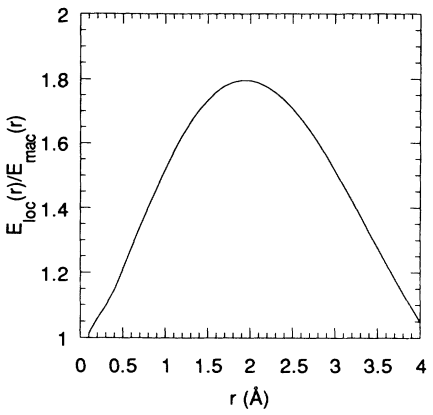

FIG. 9. Local-field enhancement for a Coulomb field in O_2 in real space.

CONCLUSIONS

We have reported enhancements in physical quantities due to local fields for four solids obtained in different manners. The behavior of the enhancements is different for each solid, but shows a common shape which includes an increase at low momentum and a peak at intermediate momentum. The values obtained are consistent with theoretical calculations. The results indicate the local fields of moderate wave vector can be much stronger than would be expected from the Clausius-Mossotti relation.

ACKNOWLEDGMENTS

Work was supported in part by NSF Grant No. DMR 88-19052. We would like to thank other members of our group, R. Carson, D. Husk, S. Velasquez, E. Benitez, and D. Li, for helpful discussions.

[1]O. F. Mossotti, Mem. di Mathem. e di Fisica in Modena **24**, 49 (1850).

[2]R. Clausius, *Die Mechanische Behandlung der Electricität* (Vieweg, Braunschweig, 1879), Vol. II, p. 62.

[3]H. A. Lorentz, Ann. Phys. **9**, 641 (1880).

[4]L. Lorenz, Ann. Phys. **11**, 70 (1880).

[5]A. C. Sinnock and B. L. Smith, Phys. Rev. **181**, 1297 (1969).

[6]S. R. Nagel and T. A. Witten, Phys. Rev. B **11**, 1623 (1975).

[7]C. Tarrio and S. E. Schnatterly, Phys. Rev. Lett. **66**, 644 (1991).

[8]P. C. Gibbons, J. J. Ritsko, and S. E. Schnatterly, Rev. Sci. Instrum. **46**, 1546 (1975).

[9]C. Tarrio, S. E. Schnatterly, and E. L. Benitez, Rev. Sci. Instrum. **61**, 2704 (1990).

[10]R. Wyckoff, *Crystal Structures* (Wiley, New York, 1963), Vol. 1.

[11]J. R. Fields, Ph. D. thesis, Princeton University, 1975.

[12]P. Livins, T. Aton, and S. E. Schnatterly, Phys. Rev. B **38**, 5511 (1988).

[13]D. Y. Smith, in *The Handbook of Optical Constants,* edited by E. R. Palik (Academic, Orlando, 1986), Chap. 3.

[14]G. R. Alms, A. K. Burnham, and W. D. Flygare, J. Chem. Phys. **63**, 3321 (1975).

[15]A. Skerbele and E. N. Lassettre, J. Chem. Phys. **49**, 305 (1970).

[16]N. Oda and T. Osawa, J. Phys. B **14**, L563 (1981).

[17]E. Fainelli, R. Camilloni, G. Petrocelli, and G. Stefani, Nuovo

Cimento D **9**, 33 (1987).
[18]H. P. Kelley, Phys. Rev. **182**, 84 (1969).
[19]E. Boursey *et al.*, Phys. Rev. Lett. **41**, 305 (1978).
[20]E. N. Lassettre, S. M. Silverman, and M. E. Krasnow, J. Chem. Phys. **40**, 1261 (1964).
[21]U. Rossler, in *Rare Gas Solids,* edited by M. L. Klein and J. A. Venables (Academic, New York, 1974), Vol. 1, Chap. 8.
[22]C. E. Moore, *Atomic Energy Levels* (National Bureau of Standards, Washington, D.C., 1971), Vol. I, p. 212.
[23]R. Haensel *et al.*, Phys. Rev. Lett. **23**, 116 (1969).
[24]M. Skibowski (unpublished).